THE JOURNAL OF PHYSICAL CHEMISTRY C
A JOURNAL OF THE AMERICAN CHEMICAL SOCIETY

pubs.acs.org/JPCC

Article

Identification of a Stable B_2H_2 Intermediate in the Decomposition of $Zr(BH_4)_4$ on the Pd(111) Surface

Ravi Ranjan, Morgan Redington, Ayoyele Ologun, Eva Zurek, Daniel P. Miller,* and Michael Trenary*

Cite This: *J. Phys. Chem. C* 2024, 128, 12414−12426

Read Online

ACCESS | Metrics & More | Article Recommendations | Supporting Information

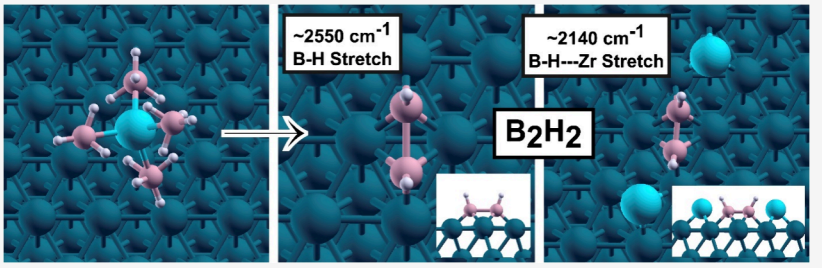

ABSTRACT: Tetrakis(tetrahydroborato)zirconium(IV), $Zr(BH_4)_4$, is a volatile compound that has been widely used as a single-source precursor to grow carbon-free thin films of zirconium diboride by chemical vapor deposition (CVD) on a wide range of substrates that include oxides, semiconductors, and metals. However, the basic surface chemistry of the compound that underlies the initial stages of the CVD process is largely unknown for any substrate. We studied the adsorption and decomposition of $Zr(BH_4)_4$ on a Pd(111) surface with the experimental techniques of reflection absorption infrared spectroscopy (RAIRS), temperature-programmed reaction spectroscopy (TPRS), and X-ray photoelectron spectroscopy (XPS) and with density functional theory and first-principles molecular dynamics simulations. After exposing Pd(111) at 90 K to $Zr(BH_4)_4$ (g), a RAIR spectrum was obtained that closely matched that of the pure compound, indicating that it adsorbs without dissociation at 90 K. However, upon heating to 200 K the RAIR spectrum undergoes dramatic changes indicating that a new surface species is formed that retains both terminal B−H bonds and bridging metal−H−B bonds, as indicated by B−H stretches in the ranges of 2563−2540 and 2143−2135 cm^{-1}, respectively. Hydrogen desorption is first observed at around 178 K and the presence of a stable hydrogen-containing surface intermediate is revealed by additional H_2 desorption peaks at 330 and 426 K. A combination of theoretical methods reveals that BH adsorbed at a 3-fold hollow site on the Pd(111) surface is the most stable species, but once formed two BH molecules can dimerize to form HBBH. A stable configuration for B_2H_2 is achieved through formation of B−H---Zr bridge bonds with a Zr atom located at one or both ends of a B_2H_2 molecule. Calculated vibrational frequencies and intensities provide an excellent match with the experimental RAIR spectra.

1. INTRODUCTION

Surface chemical reactions play a central role in important thin-film growth methods such as atomic layer deposition (ALD) and chemical vapor deposition (CVD).[1−5] A detailed understanding at the atomic and molecular level of the surface chemistry that underlies such methods is needed to develop a more rational approach to optimizing and expanding the application of thin-film growth processes. The obvious and vast technological importance of thin films has led to applied research efforts to improve deposition methods, while relatively little basic research is being devoted to the surface reaction mechanisms involved. This is despite the existence of powerful experimental techniques that can provide such information.

Previous work has shown that the compounds $Zr(BH_4)_4$ and $Hf(BH_4)_4$ can be used to deposit highly conformal and stoichiometric ZrB_2 and HfB_2 films at low growth temperatures.[6−16] These compounds, zirconium and hafnium tetrakis-(tetrahydroborato), often referred to simply as the borohydrides, are solids at room temperature but with high vapor pressures that make them convenient precursors for boride film growth. As the chemistry of Zr and Hf are quite similar, conclusions reached for growth of HfB_2 films from $Hf(BH_4)_4$ are highly relevant to ZrB_2 film growth from $Zr(BH_4)_4$. In a series of papers, the research groups of Abelson and Girolami have explored various properties of primarily HfB_2 films grown from $Hf(BH_4)_4$.[9−18] They have found that while amorphous films are produced at 200 °C, crystalline and even epitaxial films are formed at higher temperatures. One of their

Received: April 9, 2024
Revised: June 19, 2024
Accepted: July 5, 2024
Published: July 22, 2024

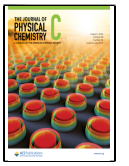

https://doi.org/10.1021/acs.jpcc.4c02327
J. Phys. Chem. C 2024, 128, 12414−12426

significant findings is that highly conformal films can be formed under appropriate conditions. Furthermore, the growth rate from a single source precursor, such as $Hf(BH_4)_4$, can be considerably higher than is typically possible with ALD.[19] If the reaction probability for the precursor with the surface is too high for conformal growth, then inhibitors can be added to decrease the surface reaction probability. A detailed understanding of these surface processes implies that it may be possible to more widely achieve conformal growth, while retaining the advantages of single-precursor CVD methods over ALD.

The interest in these thin films stems from the unique properties of transition metal diborides, including TiB_2, ZrB_2, and HfB_2, which are extremely hard, high melting point metals with high electrical conductivity. They find applications as hard, refractory coatings and have been explored as diffusion barriers in microelectronics.[20−22] Other remarkable discoveries among the diborides include finding that MgB_2 becomes superconducting at 39 K[23] and that OsB_2 has an extremely high bulk modulus, suggesting it might be a new ultrahard material,[24] although this was later disputed.[25] Because of a good lattice match between GaN and ZrB_2, epitaxial films of ZrB_2 on Si substrates have been explored as buffer layers for the growth of GaN on Si.[26−34]

The numerous previous studies of the growth of transition metal diborides from borohydride precursors leave important questions unanswered. Mass spectrometry showed that the excess boron and hydrogen are removed as diborane (B_2H_6) and H_2 according to the equation[8]:

$$Zr(BH_4)_4(g) \rightarrow ZrB_2(s) + B_2H_6(g) + 5H_2(g) \quad (1)$$

This net reaction must necessarily occur by multiple unknown elementary steps. Unlike the strong covalent bonding between Zr and B in the diboride, in $Zr(BH_4)_4$ there is no direct Zr−B bonding. Instead, the BH_4 groups bond to the central Zr atom via three B−H---Zr bridge bonds from each BH_4 group, as shown in Figure 1. These bridge bonds are an example of the three-center two-electron bonding that is a distinctive feature of boron chemistry. One goal of the present study was to determine if this aspect of boron chemistry would play a role in the surface reactions of borohydride CVD precursors.

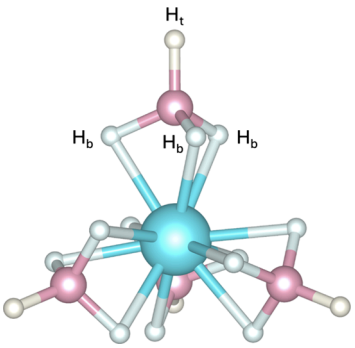

Figure 1. Optimized gas-phase structure of tetrakis(tetrahydroborato)zirconium(IV), $Zr(BH_4)_4$. The Zr atom is colored cyan, B atoms are colored pink, bridging H (H_b) atoms are colored white, and terminal H (H_t) atoms are cream colored. Solid lines indicate bonds.

In contrast to the numerous past studies of diboride film growth from borohydride precursors, the work described here focuses on the adsorption of $Zr(BH_4)_4$ on a Pd(111) surface and its decomposition pathways. Despite the importance of surface reactions in film growth, little consideration has been given to the nature of the substrate used to grow MB_2 films from $M(BH_4)_4$, where the earliest examples were of films grown on materials such as glass, sapphire, quartz, silicon, or iron foils.[6−8] To align computational and experimental results on surface reactions, it is desirable to use well-characterized single crystals so that the models of surface atomic structure assumed in the computations accurately represent the surface structure used in the experiments. We chose a metal surface for this study because reflection absorption infrared spectroscopy (RAIRS) has high sensitivity for molecular adsorbates only for metallic surfaces. As palladium is generally a good dehydrogenation catalyst, it may promote the first stages of the decomposition process and thereby facilitate diboride film growth at lower temperatures. The experiments have been conducted on a clean well-ordered single crystal of Pd(111) using the surface science methods of RAIRS and X-ray photoelectron spectroscopy (XPS). The RAIRS results reveal that one or more stable intermediates form that feature both terminal B−H bonds as well as B−H---metal bridging bonds. The first-principles computations reveal that BH is by far the most stable B_xH_y species on the Pd(111) surface. However, BH can dimerize to form an HBBH species, which is stabilized through interaction with surface Zr atoms to form B−H---Zr bridge bonds. The calculated frequencies and intensities for BH, HBBH, and Zr−HBBH−Zr together provide good agreement with the experimental RAIR spectra. A recent related computational study considered the decomposition pathways of $Hf(BH_4)_4$ and $Zr(BH_4)_4$ to understand the early events in the CVD growth of MB_2 thin films.[35] However, that study did not consider surface reactions. In the case of ZrB_2 film growth, after the initial decomposition takes place, subsequent growth necessarily occurs on a ZrB_2 surface. To explore the surface chemistry of the later stages of film growth, we are conducting similar studies to those reported here on a $ZrB_2(0001)$ surface, which is a reflective metal suitable for RAIRS.[36−38]

In many cases, stable intermediates that form on metal surfaces are also found in organometallic complexes. In the well-developed field of metalloborane chemistry,[39−42] there are numerous compounds that contain both boron−metal and B−H---M bridge bonds. While much of the focus of metalloborane chemistry is on the interaction of boron hydride cluster compounds with metals, complexes with various diboranes are also known.[43] However, the high stability of the BH species on Pd(111), and its propensity to form B_2H_2 stabilized on the surface and engaged in B−H---Zr bridge bonds, represents distinctly different chemistry than is generally observed in metalloboranes.

2. METHODS

2.1. Experimental. All experiments were carried out in a stainless steel ultrahigh vacuum (UHV) chamber with a base pressure of 1×10^{-10} Torr. The chamber is equipped with an ion gun for Ar^+ sputtering (Physical Electronics, PHI 04-161), a Fourier transform infrared (FTIR) spectrometer (Mattson Instruments, RS-10,000), a hemispherical electron energy analyzer (VG Microtech, CLAM 2) with a dual Mg/Al anode X-ray source, reverse view low energy electron diffraction (LEED) optics (Princeton Research Instruments, RVL 8-120SH), and a quadrupole mass spectrometer (UTI

https://doi.org/10.1021/acs.jpcc.4c02327
J. Phys. Chem. C 2024, 128, 12414−12426

100 C) for temperature-programmed reaction spectroscopy (TPRS).[44,45] All RAIR spectra were taken with 1024 scans and 4 cm^{-1} resolution. The XPS spectra were obtained using Mg Kα radiation and pass energies of either 50 or 100 eV. Although we used the same XPS spectrometer for earlier studies of a $ZrB_2(0001)$ single crystal using a pass energy of 50 eV,[37,46] the sensitivity and resolution of the spectrometer has degraded with time.

The Pd(111) single crystal was spot-welded to two tantalum wires mounted on a liquid nitrogen cooled sample holder. A type K thermocouple was spot-welded to the top edge of the crystal for temperature measurements. The sample could be resistively heated to 1200 K and cooled with liquid N_2 to 90 K. The Pd(111) surface was prepared by Ar^+ bombardment (1 keV, 5 μA) and annealing to 1200 K in UHV. The cleanness of the surface was verified by XPS and LEED.

$Zr(BH_4)_4$ was synthesized by the reaction between $LiBH_4$ and $ZrCl_4$ in the absence of solvent[47]:

$$ZrCl_4(s) + 4LiBH_4(s) \rightarrow Zr(BH_4)_4(s) + 4LiCl(s)$$

The method used here mainly follows the procedure described by Haaland et al.[48] Zirconium tetrachloride (anhydrous) and lithium borohydride (≥90%) were purchased from MilliporeSigma and used for synthesis without purification. The sample was verified to be pure by its infrared spectrum and was stored in a glass bottle in a refrigerator for further use.[48−52]

The $Zr(BH_4)_4$ exposures were performed by opening a leak valve and backfilling the chamber and are reported in units of Langmuir, where 1 L = 1×10^{-6} Torr s. The pressure measured during exposures was based on uncorrected ion gauge readings. The ion gauge sensitivity is calibrated for N_2 and sensitivity is likely quite different for $Zr(BH_4)_4$. Ko et al. noted that ionization efficiency for a molecule scales with the number of electrons, and provided a simple equation for estimating ionization efficiency, which yields an ionization efficiency of 3.7 for $Zr(BH_4)_4$ relative to CO, which should be nearly the same as for N_2.[53] Summers found a linear correlation between ion gauge sensitivity and molecular polarizability.[54] Although an experimental value for the molecular polarizability for $Zr(BH_4)_4$ is apparently not known, we used density functional theory calculations to obtain a theoretical value, which is a factor of 23 higher than that of N_2. If the relative ion gauge sensitivity differs by the same factor, then a nominal 300 L exposure corresponds to only an actual 13 L exposure.

2.2. Computational. Periodic calculations were performed using the Vienna Ab Initio Simulation Package (VASP)[55] with the optPBE-vdW[56,57] density functional, which accounts for London dispersion forces through an augmented nonlocal correlation functional. A plane-wave basis set energy cutoff of 500 eV was used in the geometry optimizations, first-principles molecular dynamics (FPMD), nudged elastic band (NEB),[58,59] and single-point calculations. The projector augmented wave (PAW) method[60,61] was used to treat the core states, as implemented within VASP. Due to the large size of the simulation cell, only the gamma-point was used in the periodic geometry optimizations. All atoms were allowed to relax fully within the surface−adsorbate systems in the geometry optimizations and NEB calculations, except for the bottom two layers of the four-layer 120-atom Pd(111) surfaces, which were kept fixed at the experimental bulk lattice constant for Pd (3.89 Å). As expected, in the relaxed structure for the clean Pd(111) surface the interlayer distance between the top and second layer and the second and third layer expand relative to the bulk interlayer spacing. The experimental binding energy of 1/2 H_2 to Pd(111) is reported in the literature to be −0.49 eV[62] and our computational methodology involving optPBE-vdW calculates the 1/2 H_2 adsorption to be −0.46 eV, showing excellent agreement. Single point calculations on optimized structures were performed to obtain Bader charges and charge density difference (CDD) isosurfaces. The CDD isosurfaces were calculated by subtracting the clean Pd(111) surface charge density, free zirconium charge density, and/or BH_4, BH_3, BH_2, BH, or B_2H_2 species' collective charge density from the total system charge density. The unit cell dimensions used with the Pd(111) surface were 13.75 Å × 14.29 Å × 30.00 Å, with the z-axis being large to ensure sufficient vacuum space to prevent unwanted interactions between periodic images. Gas-phase calculations were performed on isolated molecules, atoms, or molecular fragments, as appropriate, within a box of the same size employed to model the surface−adsorbate system. The FPMD simulation was performed with the NVT ensemble (constant number of particles, constant volume, constant temperature), Nosé−Hoover thermostat,[63,64] a 1.0 fs time step, and a temperature of 200 K. In the FPMD simulation of $Zr(BH_4)_4$ at 200 K, a two-layer Pd(111) surface was used. The climbing image NEB method was used to obtain saddle points to approximate the transition states in the dissociation of hydrogen from $Zr(BH_4)_1$ into Zr, B, and 4H atoms on Pd(111).

Crystal orbital Hamiltonian populations (COHP) were calculated using LOBSTER[65] from VASP geometry optimized systems and their wave functions were generated using a Monkhorst−Pack k-grid of 4 × 3 × 2. The negative integrated crystal orbital Hamiltonian populations (−iCOHP) were used to determine bond strengths. The structures used in LOBSTER were selected from the geometry optimized structures to include only the adsorbates and the first layer of Pd atoms.

The Pd(111) surface is a large reservoir of electrons and it can readily accept or donate electrons to the adsorbate, which makes the addition or removal of charge on surface species nontrivial. Therefore, we postulated that calculations on neutral models would yield results that were in-line with those obtained for models whose charges were chosen to reflect the formal charge of the adsorbate. To ensure our focus on uncharged models was sound, a benchmark was performed comparing the relative energies and B−H bond lengths in the Pd(111) adsorbed Zr+BH+3H versus $Zr+BH+3H^{3+}$ systems along with the Pd(111) adsorbed $ZrBH_4$ versus $ZrBH_4^{3+}$ systems. The B−H bond lengths were identical in the charged and neutral BH and BH_4 species, and the relative energy of adsorbed Zr+BH+3H versus $ZrBH_4$ with and without included charges only differed by 0.02 eV/adsorbate atom. Unfortunately, the software package (VASP) that we used allows for charged systems to be computed, but does not allow for charges to be placed on particular atoms nor include charge in a simple user-friendly fashion.

The binding energies (eq 2) and formation energies (eq 3) discussed in the computational section were calculated using the following equations:

https://doi.org/10.1021/acs.jpcc.4c02327
J. Phys. Chem. C 2024, 128, 12414−12426

$$\text{Binding Energy} = [\text{Surface} - \text{Adsorbate System Energy}] - [\text{Pd(111) Surface Energy}] - [\text{Adsorbate Energy}] \quad (2)$$

$$\text{Formation Energy} = [\text{Surface} - \text{Adsorbate System Energy}] - [\text{Pd(111) Surface Energy}] - z^*[\text{Zr Atom Energy}] - b^*[\text{B Atom Energy}] - h^*[\text{H Atom Energy}] \quad (3)$$

where z, b, and h are the number of Zr, B, and H atoms, respectively, in the modeled system, and the energies employed were those of isolated atoms.

Gas-phase density functional theory calculations were also performed using Gaussian16[66] to obtain vibrational frequencies, total infrared intensities, and intensities proportional to the square of the z-component (the surface normal) of the dipole derivatives as the latter corresponds to the experimental RAIRS intensities. The PBE generalized gradient approximation (GGA) functional and Def2-TZVPP basis set were used in the Gaussian vibrational frequency calculations on VASP geometry optimized structures of $Zr(BH_4)_4$, and hypothesized dissociation products $Zr(BH_4)_1$, $Zr(BH_3)_2$, $Zr(BH_3)_1$, $Zr(BH_2)_1$, Zr+BH adj, Zr+BH sep (BH), BH_4, BH_3, B_2H_2, B_2H_2−Zr, B_2H_2−2Zr, B_2H_4, and B_2H_6 adsorbed on the Pd(111) surface. The VASP geometry optimized structures on Pd(111) imported into Gaussian were selected to include only first layer Pd atoms that ensure hollow sites, bridge sites, and top sites were accounted for.

3. RESULTS

3.1. RAIRS and TPRS. RAIR spectra for 300 and 500 L exposures of zirconium borohydride to the Pd(111) crystal at 90 K are shown in Figure 2. For both exposures, the most intense peaks are assigned to terminal B−H stretches (2571−2573 cm^{-1}), bridging B−H---Zr stretches (2173-2197 cm^{-1}), and H−B−H bending modes (1225−1232 cm^{-1}). For the 500 L exposure, several weaker peaks are also observed. The RAIRS peaks observed here are compared in Table 1 with reported values for $Zr(BH_4)_4$ in the gas phase, trapped in an N_2 matrix, and in the solid phase. The excellent agreement, particularly with solid $Zr(BH_4)_4$, indicates that $Zr(BH_4)_4$ adsorbs non-dissociatively at 90 K and forms a multilayer structure like that in the molecular solid. The biggest discrepancy is for the most intense peak for the 500 L exposure at 1232 cm^{-1}, which is 14 cm^{-1} higher than in the solid. For the 300 L exposure, it is at the same position as in a solid N_2 matrix. In their normal-mode analysis of the IR and Raman spectra of $Zr(BH_4)_4$, Smith et al. found from the potential energy distribution of the internal coordinates that the mode giving rise to the 1217 cm^{-1} peak consisted of 27% Zr−H_b stretch, 61% H_tBH_b bend, and 23% H_bBH_b bend, where H_b and H_t refer to bridging and terminal hydrogens, respectively.[67]

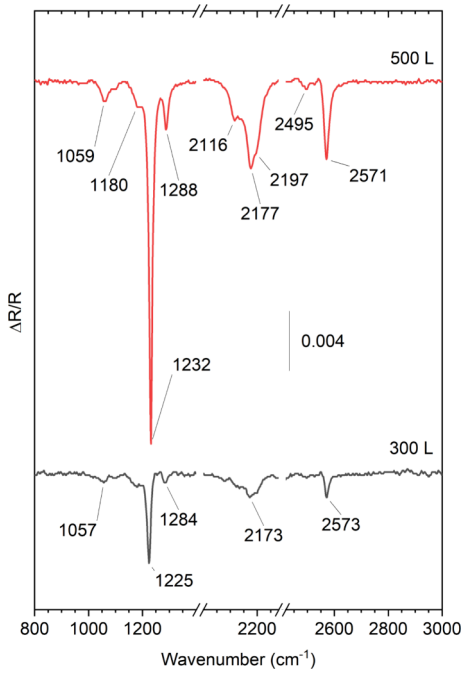

Figure 2. RAIR spectra after nominal exposures of 300 and 500 L of $Zr(BH_4)_4$ to Pd(111) at 90 K.

Table 1. Comparison of Frequencies (in cm^{-1}) for a 500 L Exposure of $Zr(BH_4)_4$ to the Pd(111) Surface at 90 K with Values from the Literature[a]

N_2 matrix (14 K)[48]	gaseous[68]	solid (77 K)[67]	Pd(111) (90 K)	assignment
2590	2575s	2580 (sh)	---	νB−H_t
---	---	2569m	2571s	νB−H_t
---	---	2563m	---	νB−H_t
2500	2493w	---	2495w	1218 + 1288 = 2506
2430	2431w	---	---	2 × 1218 = 2436
2350	---	---	---	---
2320	---	---	---	---
2210	2194s	2199 (sh)	2197 (sh)	νB−H_b
2175	---	2171m	2177s	νB−H_b
2110	2133s	2107m	2116m	νB−H_b
1600	---	---	---	---
1295	1288w	---	1288m	δH−B−H
1225	1218vs	1217s	1232vs	δH−B−H
1190	---	1185 (sh)	1180m	δH−B−H
1065	1034w	1058mw	1059m	δH−B−H
670	---	581w	---	νZr−H_b
525	560vw	547w	---	νZr−H_b
---	507s	504s	---	νZr−BH_4
---	213m	216mw	---	δBH_4−Zr−BH_4

[a]Relative intensities are indicated by s = strong, m = medium, w = weak, and v = very. (sh) = shoulder.

Figure 3 shows RAIR spectra after a 400 L exposure of $Zr(BH_4)_4$ to Pd(111) at 90 K and after annealing to the indicated temperatures. The 150 K spectrum shows a small decrease in peak intensities, but otherwise is almost the same as the 90 K spectrum. Annealing to 200 K causes significant changes, most prominently the complete loss of the 1230−1228 cm^{-1} peak, leaving behind only two peaks at 2563 and 2143 cm^{-1}. These two peaks lose intensity and are red-shifted after the 250 and 300 K anneals, but are absent after annealing to temperatures of 350 K and above. In the complementary TPRS experiments shown in Figure 4, three H_2 desorption peaks at 178, 330, and 426 K are observed. The 178 K peak is attributed to fragmentation of the parent molecule. The peak at 330 K is close to that of recombinative desorption of H_2 from the clean Pd(111) surface implying that adsorbed H

https://doi.org/10.1021/acs.jpcc.4c02327
J. Phys. Chem. C 2024, 128, 12414−12426

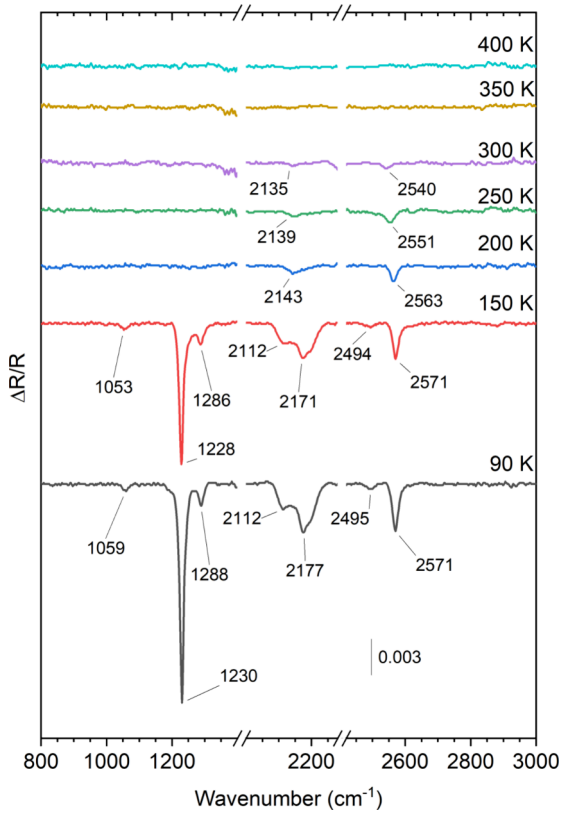

Figure 3. RAIR spectra after a 400 L exposure of $Zr(BH_4)_4$ to Pd(111) at 90 K and after annealing to the indicated temperatures. After annealing, the crystal was cooled back to 90 K before the spectra were acquired.

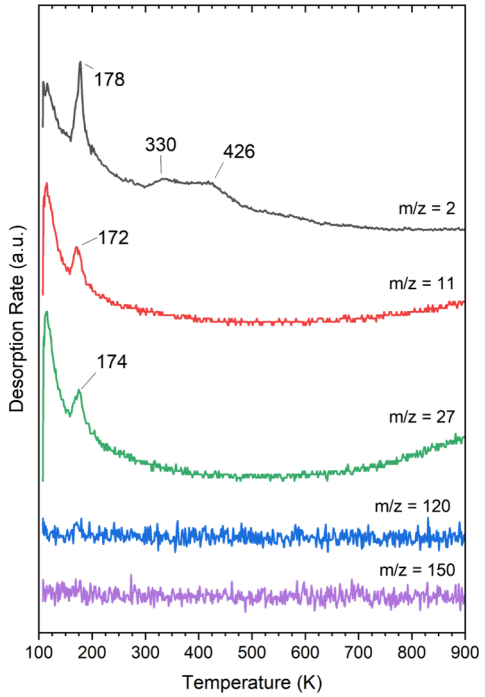

Figure 4. TPRS results after a 500 L exposure of $Zr(BH_4)_4$ to Pd(111) at 90 K. The mass-to-charge ratios (m/z) measured were 2, 11, 27, 120, and 150 amu. The hydrogen signal was scaled by 1/100.

atoms were already present due to decomposition of $Zr(BH_4)_4$ at lower temperatures. Conversely, the 426 K H_2 peak must be due to reaction-limited desorption, implying the presence of a hydrogen-containing surface species up to this temperature. Desorption of the parent molecule, corresponding to m/z ratios of 120 and 150, was not directly detected by TPRS. However, the B_2H_6 (m/z = 27) and B (m/z = 11) peaks at 174 and 172 K are assigned to fragments of the parent molecule desorption.

3.2. XPS. Figure 5 shows XPS spectra after exposing 500 L of $Zr(BH_4)_4$ to Pd(111) at 90 K and then annealing to the

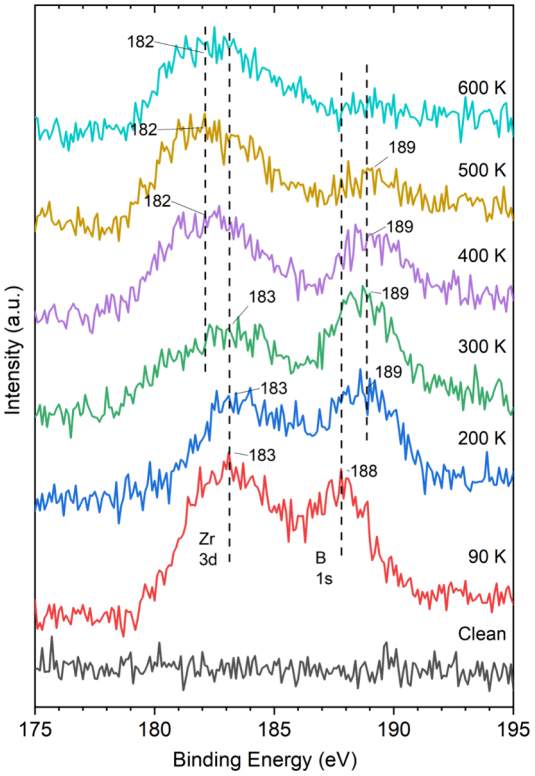

Figure 5. XPS spectra in the B 1s/Zr 3d region as a function of annealing temperature after a 500 L $Zr(BH_4)_4$ exposure to Pd(111) at 90 K.

indicated temperatures. The clean Pd(111) surface does not show any peaks from 170 to 200 eV. Molecularly adsorbed $Zr(BH_4)_4$ at 90 K has a Zr 3d peak at 183 eV and a B 1s peak at 188 eV. At the pass energy used, 100 eV, the Zr $3d_{5/2}$, $3d_{3/2}$ peaks, which are separated by 2.4 eV, are not resolved. The $Zr(BH_4)_4$-layer thickness, d, at 90 K can be estimated from the attenuation of the Pd $3d_{5/2}$ peak using eq 4,

$$\frac{I}{I^0} = \exp\left(-\frac{d}{\lambda\cos\theta}\right) \tag{4}$$

where I^0 is the Pd $3d_{5/2}$ peak area of the clean Pd(111) surface, I is the peak area following $Zr(BH_4)_4$ adsorption, and λ is the inelastic mean free path of the electrons in the $Zr(BH_4)_4$ layer. In this equation, θ is the angle between the surface normal and the analyzer, which in our case is approximately zero ($0 \pm 15°$). We used the calculated inelastic mean free path λ = 32 Å for 1000 eV electrons in ZrO_2 and assumed the same value for electrons in solid $Zr(BH_4)_4$.[69] This yields d = 12 Å, which would correspond to a few layers of $Zr(BH_4)_4$. After annealing to 200 K, the molecule decomposes with the boron peak moving to a higher binding energy of 189 eV where it remains for further annealing temperatures but decreases in intensity

https://doi.org/10.1021/acs.jpcc.4c02327
J. Phys. Chem. C 2024, 128, 12414−12426

above 400 K and is just barely visible after annealing at 600 K. After annealing to 400 K and above, the Zr peak shifts to a lower binding energy of 182 eV.

Figure 6 shows an XPS survey spectrum after CVD growth of a ZrB_2 film formed by an 1800 L exposure of $Zr(BH_4)_4$ to

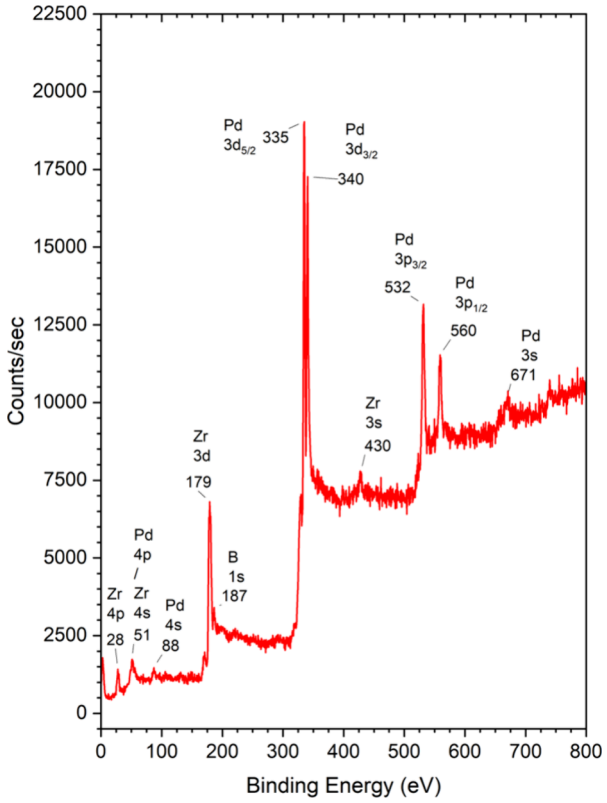

Figure 6. XPS spectrum from 0 to 800 eV after exposing 1800 L of $Zr(BH_4)_4$ to Pd(111) at 773 K.

the Pd(111) crystal held at 773 K. Previous work has indicated that at this temperature a crystalline ZrB_2 film should form.[9] No elements other than Zr, B, or Pd are visible in the spectrum. In particular, no carbon or oxygen contamination is detected. This is in contrast to what has been reported in conventional CVD growth experiments where oxygen contamination is observed.[6−9] Table 2 lists the peaks and their binding energies from Figure 6. Using eq 4 again with an assumed inelastic mean free path of 32 Å, we calculated a ZrB_2 layer thickness of 18 Å.

Figure 7 shows the XPS spectra obtained with pass energies of 100 and 50 eV following exposure of 1800 L of $Zr(BH_4)_4$ to the Pd(111) surface at 773 K. At a pass energy of 50 eV, the Zr $3d_{5/2}$ peak at 179 eV can be resolved from the Zr $3d_{3/2}$ peak at

Table 2. XPS Peak Assignments and Positions of Zr, B, and Pd for a 1800 L Exposure of $Zr(BH_4)_4$ to Pd(111) at 773 K

peaks	binding energy (eV)	peaks	binding energy (eV)
Zr 4p	28	Pd 4p, Zr 4s	51
Zr 3d	179	Pd 4s	88
B 1s	187	Pd $3d_{5/2}$	335
Zr 3s	430	Pd $3d_{3/2}$	340
		Pd $3p_{3/2}$	532
		Pd $3p_{1/2}$	560
		Pd 3s	671

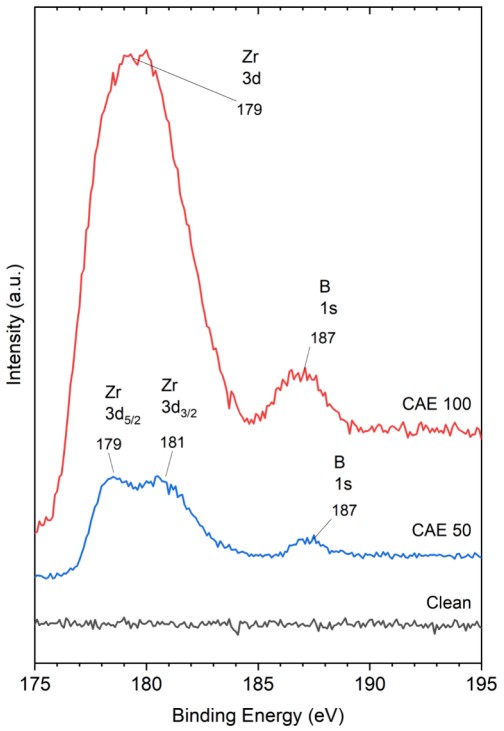

Figure 7. XPS spectra in the B 1s/Zr 3d region at pass energies of 100 and 50 eV following exposure of 1800 L of $Zr(BH_4)_4$ to Pd(111) at 773 K.

181 eV, and the B 1s peak is at 187 eV. These binding energies can be compared to our previous XPS results for a ZrB_2(0001) single crystal where the Zr $3d_{5/2}$, Zr $3d_{3/2}$, and B 1s peaks were observed at 179.2, 181.6, and 188.2 V, respectively.[46] These earlier XPS results were also obtained with a pass energy of 50 eV, and therefore at the same nominal resolution. The fact that the separation between the two Zr 3d components is less distinct here may be associated with a lower degree of crystallinity in the ZrB_2 film on Pd(111). These binding energies are 0.2 eV higher than the values we reported earlier using a different XPS system and a different ZrB_2(0001) single crystal.[70] Within the accuracy of the measurements, the ZrB_2/Pd(111) film binding energies match those of the ZrB_2(0001) surface.

In principle, the stoichiometry of the film can also be determined from XPS using the appropriate sensitivity factors for Zr and B. However, Weng et al. evaluated the accuracy in using XPS to quantify composition and concluded that the error can be as high as 15%.[71] Our previous XPS work with a ZrB_2(0001) single crystal surface was obtained with the same spectrometer used here and that crystal had a carefully measured stoichiometry of $ZrB_{2.07}$.[72] The XPS results from that crystal implied a sensitivity factor ratio of 16.4 based on the Zr $3d_{5/2}$ to B 1s peak area ratios. The areas were determined based on Gaussian fits to the peaks after a Shirley background subtraction. Interestingly, the sensitivity factor ratio using a different spectrometer was 16.2 for the same angle that we used of 54.7° between the analyzer and X-ray source.[73] Using a sensitivity factor ratio of 16.4 implies the stoichiometry of our film based on the results in Figure 7 is $ZrB_{1.7\pm0.3}$, where an uncertainty of 15% is assumed. This is also the error associated with measuring the peak areas from the 50 eV pass energy spectrum in Figure 7.

https://doi.org/10.1021/acs.jpcc.4c02327
J. Phys. Chem. C 2024, 128, 12414−12426

3.3. Computation. The pathway for dissociation of $Zr(BH_4)_4$ on the Pd(111) surface was explored computationally by calculating energies of the parent molecule and possible molecular fragments as adsorbed on the Pd(111) surface. In considering the sequential loss of BH_4 units according to the equation $Zr(BH_4)_4 \rightarrow Zr(BH_4)_{4-n} + nBH_4$, it was found that $Zr(BH_4)_{4-n}$ was stably adsorbed and that BH_4 would dissociate to form adsorbed BH + 3H (BH boron atom adsorbed to H_{hcp} site and three hydrogen atoms adsorbed to H_{fcc} sites on the surface) as the most stable product. In particular, the formation of BH from $Zr(BH_4)_4$, $Zr(BH_4)_3$, $Zr(BH_4)_2$, and $Zr(BH_4)_1$ releases 2.68, 1.28, 1.01, and 0.94 eV, respectively (Supporting Information (SI) Section S2). The results from the FPMD simulations presented in Figure 8, also support $Zr(BH_4)_4$ decomposition by sequential loss of BH_4 units into BH units, but with one lingering $Zr-BH_4$ after 12 ps at 200 K. However, even after 12 ps, this FPMD run is not yet fully equilibrated, as evidenced by the continual decrease in the energy during the simulation time (Figures S15 and S16). Visualization of the trajectory reveals that dissociation of the last remaining Zr-bound BH_4 unit has yet to occur. To further explore the decomposition of the final $Zr(BH_4)_1$ species obtained in the FPMD, nudged elastic band (NEB) calculations and conventional geometry optimizations were used to obtain approximate transition states/saddle points and energy minima, respectively, as presented in Figure 8b. The low activation energies of approximately 0.27, 0.10, and 0.17 eV for loss of the first, second, and third H, respectively, from $Zr(BH_4)_1$ make it kinetically feasible to reach the final configuration of BH adsorbed at an hcp (hexagonal close-packed) 3-fold hollow site and separated from the Zr (Zr+BH sep), with Zr+BH sep being 0.24 eV more stable than its adjacent version, called Zr +BH adj (see Figure 8b). The Zr+BH adj and Zr+BH sep structure models are illustrated in Figure 8c. The dissociation of BH to produce adsorbed B and H atoms is endothermic by 0.38 eV with a large (approximate) barrier of 0.91 eV, further supporting BH as a stable species on the Pd(111) surface.

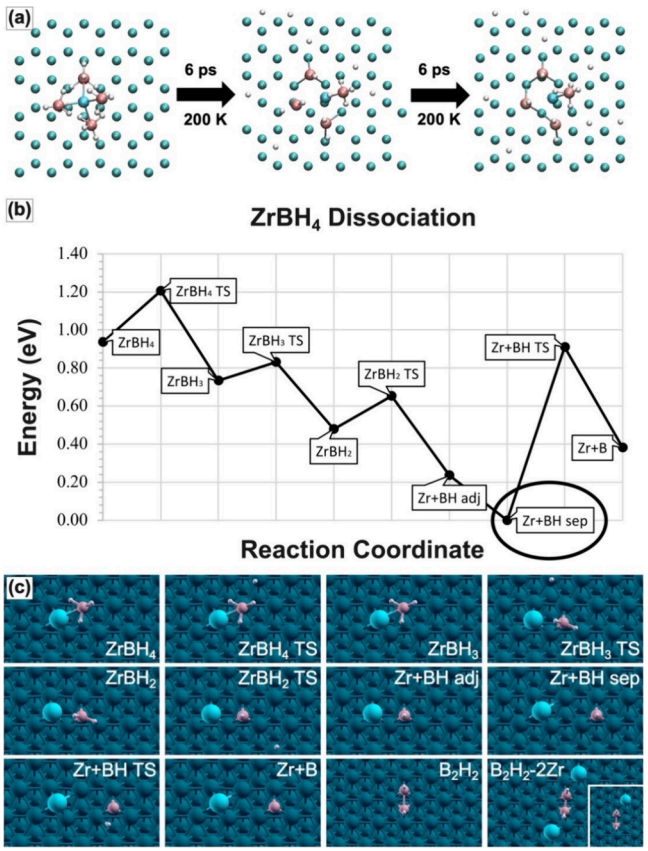

Figure 8. (a) The FPMD simulation over 12 ps at 200 K for $Zr(BH_4)_4$. Three BH units form and one $Zr(BH_4)_1$ unit is retained above the Pd(111) surface. (b) The reaction profile showing the energies of each adsorbed species and the approximate transition state energies between species in the dissociation of $Zr(BH_4)_1$ to form one Zr, one B, and four H atoms adsorbed on Pd(111). The most stable structure was observed to be BH adsorbed on Pd(111) separated from Zr, labeled Zr+BH sep, which is more stable than Zr+BH at adjacent sites, Zr+BH adj. All energies are relative to the energy of the most stable structure, Zr+BH sep. (c) The structures of the various adsorbed species and transition states from (b). The structures of B_2H_2 and B_2H_2-2Zr on Pd(111) are also shown, with B_2H_2-Zr in the bottom-right inset. The hydrogen, boron, zirconium, and palladium atoms are colored white, pink, cyan, and teal, respectively.

Inspection of the energies of various Zr/B/H adsorbed species shows that in the reactions $Zr(BH_4)_{4-n} \rightarrow nBH_4 + Zr$, as n increased, the binding energy of $Zr(BH_4)_{4-n}$ also increased. The formation energies of the $Zr(BH_4)_{4-n}$ species also follows this trend so long as the energies are divided by the number of BH_4 units present. The equations for how the binding and formation energies were calculated are given in the computational methods section above. Thus, the Pd(111) adsorbed binding energies decrease in the order $Zr(BH_4)_1 > Zr(BH_4)_2 > Zr(BH_4)_3 > Zr(BH_4)_4$. The Zr+BH adj and Zr+BH sep species have the most stable binding energy compared to $Zr(BH_4)_1$, $Zr(BH_3)_1$, and $Zr(BH_2)_1$. Zr and B atoms were found to adsorb more strongly to hcp 3-fold hollow sites while H atoms bonded more strongly to fcc (face-centered cubic) 3-fold hollow sites (H_{fcc}). For BH_4, BH_3, BH_2, and BH, the most stable configuration was with the boron atom above the hollow sites. Bader charges show that the charge transfer increases between the Pd(111) surface and the various adsorbed structures as they approach full dissociation and form BH units, with Zr+BH donating 1.5-1.6 e to the surface. The full analysis of energetics, binding site preferences, bond lengths, and Bader charges are provided in the SI, Tables S5−S14.

Given the stability of BH on the Pd(111) surface, BH dimerization was considered. This process was found to form a B_2H_2 unit stably adsorbed on Pd(111) at an energetic minimum with all real frequencies (as computed using a molecular model within, but with some of the surface atoms included). B_2H_2 is also capable of forming B_2H_2-2Zr through B−H---Zr bridging interactions that are unaltered by the Pd(111) surface. The calculated frequencies and intensities of BH, B_2H_2, and B_2H_2-2Zr adsorbed at their respective most stable sites are given in Table 3. Both BH and B_2H_2 have calculated terminal B−H stretches about or within the range of 2563−2540 cm^{-1}, close to the experimental values. BH was calculated to vibrate at 2528 cm^{-1} when isolated entirely on the Pd(111) surface. Furthermore, although two B−H stretches are calculated for both B_2H_2 and B_2H_2-2Zr, the higher wavenumber peak of the pair has a much higher calculated RAIRS intensity, implying that only the more intense one would be observable in the experiment. Unlike the IR spectrum of $Zr(BH_4)_4$, the surface intermediate that gives rise to the 2143−2135 cm^{-1} peak does not have an observable peak in the H−B−H bending region. According to the calculated frequencies and intensities presented in the SI, this rules out surface intermediates containing BH_4, BH_3, and BH_2

https://doi.org/10.1021/acs.jpcc.4c02327
J. Phys. Chem. C 2024, 128, 12414−12426

Table 3. Computed IR Frequencies and Intensities for BH, which is the same as Zr+BH sep, B_2H_2, and B_2H_2−2Zr on Pd(111) above 1000 cm^{-1}[a]

Model system	Frequency (cm^{-1})	Total IR intensity (km/mol)	z IR intensity (km/mol)
BH	2532	85	85
B_2H_2	2554	6	4
	2564	45	45
B_2H_2−2Zr	2139	72	2
	2150	116	114

[a]Both the total intensities and the intensities based on the square of the z component of the dipole derivative are given as the latter is responsible for the experimental RAIRS intensities. Although there are two B−H stretching peaks for both B_2H_2 and B_2H_2−2Zr, only one is calculated to have enough intensity to be observable with RAIRS.

with and without Zr interactions. Instead, a species that gives a strong calculated B−H---Zr stretch is B_2H_2, with one or both BH bonds interacting with a neighboring Zr atom. All other considered species like Zr+BH adj (2260−2396 cm^{-1}, depending upon the B−H---Zr distance), B_2H_4 and B_2H_6 include frequencies between 2220 and 2500 cm^{-1}, above 2600 cm^{-1}, or below 2100 cm^{-1}, which are not observed experimentally (see SI, Section S4). Attempts made to put Zr +BH adj into an ideal geometry on Pd(111) to produce a stretching vibration close to 2143−2135 cm^{-1} with knowledge of the length necessary from B_2H_2 result in the geometry optimization pushing the BH hydrogen farther from the Zr due to the need for BH, without the B−B bond, to stand vertically along the surface normal.

As shown in Table S5, an isolated B_2H_2 has a favorable binding energy to the Pd(111) surface of −6.31 eV, and this increases through formation of one B−H---Zr bridge bond, and even more when both ends of the B_2H_2 molecule have bridge bonding to a neighboring Zr atom. Furthermore, these species give rise to a bridging B−H stretch in the range observed experimentally, but without any intense peaks in the H−B−H bending region. In the bonding configuration of B_2H_2 on Pd(111) as illustrated in Figure 8c, the two B atoms are above hollow sites. The adsorbed B_2H_2 has a lengthened B−B bond of 2.02 Å compared to 1.52 Å for gas-phase B_2H_2 shown in Figure 9. Whereas the BH bond of adsorbed BH is oriented perpendicular to the surface, in B_2H_2 the BH bonds are tilted toward the surface. In the presence of Zr atoms, the H atoms of B_2H_2 bend further toward the surface and engage in B−H---Zr bridging interactions, which does not occur when BH is adsorbed near a Zr atom. The engaging of B_2H_2 in B−H---Zr interactions also decreases the B−B bond length to 1.71 Å, and is associated with a large charge density gain between the boron atoms as seen in the B_2H_2−2Zr structure shown in Figure 9. In fact, B_2H_2−2Zr was computed to have the most negative, and favorable, binding energy out of all the investigated Zr/B/H species. The Bader charges of B_2H_2−2Zr and $ZrBH_4$ indicate that the hydrogens are hydridic while the Zr and B atoms are positively charged. On Pd(111), the Zr−H_b bond length in B_2H_2−2Zr is 2.27 Å, while it is 2.20 Å for $ZrBH_4$. These calculated values are quite similar to the experimentally determined Zr−H_b bond length in gas-phase $Zr(BH_4)_4$ of 2.21 Å.[74] The comparison indicates that B−H---Zr bridge bonds in B_2H_2−2Zr on Pd(111) are typical of hydrogen bridging bonds between boron and zirconium atoms.

The bond strengths in the various surface species were explored through LOBSTER calculations with the results

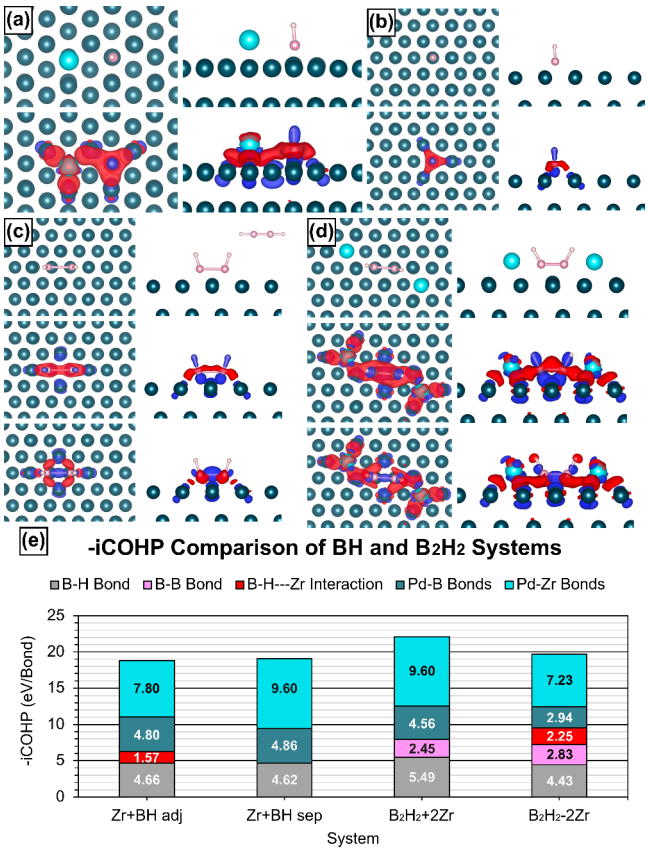

Figure 9. Structures and charge density (ρ) differences (CDD) for the given isovalues expressed in e/Å^3 of the various species on Pd(111) (a) Zr+BH adj (±0.06). (b) Zr+BH sep (±0.10). (c) B_2H_2 (±0.10). (d) B_2H_2−2Zr (±0.06). The CDDs (red = charge gain, blue = charge loss) were calculated with the following equations: (a) CDD = System (ρ) − Surface (ρ) − Zr (ρ) − BH (ρ); (b) CDD = System (ρ) − Surface (ρ) − BH (ρ); (c) [Middle] CDD = System (ρ) − Surface (ρ) − BH (ρ) − BH (ρ); (c) [Bottom] CDD = System (ρ) − Surface (ρ) − B_2H_2 (ρ); (d) [Middle] CDD = System (ρ) − Surface (ρ) − 2Zr (ρ) − BH (ρ) − BH (ρ); (d) [Bottom] CDD = System (ρ) − Surface (ρ) − 2Zr (ρ) − B_2H_2 (ρ). (e) The total −iCOHP for the Zr+BH adj, Zr+BH sep, B_2H_2+2Zr (which is B_2H_2 with two separated Zr atoms), and B_2H_2−2Zr systems. The average Pd−Zr bond strengths and Pd−B bond strengths were multiplied by three due to their binding sites being at 3-fold hollow sites. The B−B bond strengths were divided by two, and only one B−H bond and one B−H---Zr interaction were used for the totals to ensure an equal number of bonds considered to properly compare BH and B_2H_2 systems. Gas-phase B_2H_2 is illustrated in the top-right of (c). The hydrogen, boron, zirconium, and palladium atoms are colored white, pink, cyan, and teal, respectively. The bonds made between the adsorbate atoms and the underlying Pd(111) surface were removed for clarity.

presented in Figure 9 for the Zr+BH adj, Zr+BH sep, B_2H_2, and B_2H_2−2Zr systems and in Section S5. For both adsorbed $Zr(BH_4)_4$ and $Zr(BH_4)_1$, the calculated −iCOHP values are 2.23 and 2.05 eV/bond for each of the B−H---Zr interactions, calculated by adding the Zr−B and Zr−H interactions, and averaging them. Upon adsorption to Pd(111), BH_4 has its B−H bond −iCOHP value lowered to 3.98 eV/bond from 4.97 eV/bond, reflecting the weakening of the B−H bonds prior to BH_4 dissociation. This reduction in bonding interaction is also seen in B−H bonds weakening as BH_4 units leave Zr; the largest B−H bond strength in $Zr(BH_4)_4$ is 5.05 eV/bond, showing significantly more bonding character than the

https://doi.org/10.1021/acs.jpcc.4c02327
J. Phys. Chem. C 2024, 128, 12414−12426

Table 4. H−B−B Bond Angle, Boron and Zirconium Binding Sites, B−H and B−B Bond Lengths, Binding Energy (eV/BH), Formation Energy (eV/BH), and Total Bonding Strength Using −iCOHP Values (eV/BH)[a]

system	H−B−B bond angle	B binding site	Zr binding site	B−H bond length (Å)	B−B bond length (Å)	binding energy (eV/BH)	formation energy (eV/BH)	total bonding strength, −iCOHP (eV/BH)
Zr+BH adj	94°	H_{hcp}	H_{hcp}	1.22		−13.60	−18.73	18.83
Zr+BH sep	91°	H_{hcp}	H_{hcp}	1.20		−14.08	−19.00	19.08
B_2H_2+2Zr	107° [178°]	H_{hcp}/H_{fcc}	H_{hcp}	1.20 [1.17]	2.02 [1.52]	−11.58	−18.72	22.10
B_2H_2−2Zr	118°	H_{hcp}/H_{fcc}	H_{hcp}/H_{fcc}	1.25	1.71	−7.85	−18.45	19.68

[a]Zr+BH sep and B_2H_2+2Zr are the same as BH and B_2H_2 alone on Pd(111) but they include the binding energy of 1 Zr and 2 Zr, respectively, to compare to Zr+BH adj and B_2H_2−2Zr. Values given in brackets are for gas-phase B_2H_2. The equations for calculating binding energy and formation energy are given in the computational methods. The H−B−B bond angles for Zr+BH adj and Zr+BH sep were obtained by measuring with another adsorbed BH neighbor.

maximum value obtained for $Zr(BH_4)_1$, 4.14 eV/bond. The Pd−B bonds for BH and B_2H_2 have −iCOHP values of about 1.6 eV/bond, consistent with chemisorbed species. The formation of B_2H_2 is supported by calculated −iCOHP values for its B−B bond of 7.98, 4.90, and 5.66 eV/bond in the gas-phase, adsorbed to Pd(111), and when interacting with 2Zr atoms, respectively. As Zr interacts with H, the B−H bond elongates and weakens, which strengthens the B−B bond. The strong B−B bond and relative −iCOHP values of B_2H_2 supports its formation from two adsorbed BH molecules on Pd(111). Additionally, the −iCOHP values indicate that B_2H_2 gains further bonding character from the formation of B−H---Zr bonds. This −iCOHP preference for B_2H_2 formation from BH is highlighted through the column graph given in Figure 9, where the B_2H_2 and B_2H_2−2Zr total bond strengths are larger than Zr+BH sep and Zr+BH adj. B_2H_2 has stronger bonding than B_2H_2−2Zr as there is a loss in bonding to the surface upon forming B−H---Zr bridging interactions, with a decrease from 9.60 to 7.23 eV for the Pd−Zr bonds and from 4.56 to 2.94 eV for the Pd−B bonds. However, high coverage of Zr atoms and B_2H_2 would inevitably give rise to B_2H_2−2Zr and provide a B−H stretching frequency near 2150 cm^{-1}.

The calculated CDD results of Figure 9 and the figures in Section S1 provide additional insights into bonding within $Zr(BH_4)_4$ and its dissociation products on Pd(111). In $Zr(BH_4)_4$, there is a gain of electron density at the bridging hydrogens and a charge density loss on the Zr atom. The BH_4 units closest to the Pd(111) surface experience charge density loss at the boron atom but gain electron density on the hydrogen atoms and in the region between the boron atom and the underlying Pd atom, with a corresponding loss of charge density at the Pd atoms. The $Zr(BH_4)_1$ species shows similar charge reorganization to that of $Zr(BH_4)_4$ since the Zr atom charge density loss induces gain on the bridging hydrogens of the BH_4. When $Zr(BH_4)_4$ is adsorbed on Pd(111), the terminal B−H bonds lengthen from 1.19 to 1.24−1.26 Å. The bridging H---Zr and B−H distances increase from 2.16 and 1.25 Å to 2.22−2.28 Å and 1.27−1.31 Å, respectively. In $Zr(BH_4)_1$, there is charge density gain on the terminal hydrogen of BH_4, loss at the boron atom, and gain on the hydrogen closest to the Pd(111) surface. There is a significant gain in charge density between the Zr atom in $Zr(BH_4)_1$ and the underlying Pd atoms, which is indicative of chemisorption. When adsorbed on Pd(111), $Zr(BH_4)_4$ has three bridging hydrogens per BH_4 unit, which is the same as for isolated $Zr(BH_4)_4$. However, $Zr(BH_4)_1$ has two bridging hydrogens, with the third hydrogen pointing upward and the fourth hydrogen oriented toward the Pd(111) surface, which suggests that the BH_4 unit breaks apart by replacing a B−H---Zr bond with a B−H---Pd bond. This B−H---Pd interaction causes the B−H bond to lengthen to 1.34 Å compared to a bridging B−H bond length of 1.25 Å for B−H---Zr, which supports the dissociation of BH_4 into BH_3 as the first step toward BH. The bridge site for Zr and top site for BH_4 were preferred for $Zr(BH_4)_1$. An isolated adsorbed BH (Zr+BH sep) and a BH adsorbed next to a Zr atom (Zr+BH adj) are shown in Figure 9. In both cases, BH adsorbs at hollow sites and forms three Pd−B bonds with significant charge density gain. The CDD shows electron density loss at the B−H bond, consistent with a red-shift of the B−H stretch to around 2550 cm^{-1} in the experiment compared to the terminal B−H stretch of 2571 cm^{-1} in $Zr(BH_4)_4$ on Pd(111). The CDD of B_2H_2 adsorbed on Pd(111) shows that there is significant charge density gain between the boron atoms when the CDD is calculated by duplicating the charge of one BH fragment. However, when the CDD is calculated by treating B_2H_2 in its totality there is charge density loss between the two boron atoms. This shows that there is an attraction to create B−B bonds from two BH units, but that the BH units are not fully bound together, like in the linear gas-phase geometry, because B_2H_2 must reorganize charge to enhance Pd−B bonding. In B_2H_2−2Zr, the CDD isosurfaces are similar to those within the B_2H_2 without Zr, except that the B−H---Zr interactions cause charge density gain on the hydrogen and loss on the boron and zirconium. This gain of charge density on the hydrogen atoms in B_2H_2−2Zr is in stark contrast to the loss of charge density on the hydrogen in Zr+BH adj, Zr+BH sep, and B_2H_2. Although there is a gain of charge density on the hydrogen atoms of B_2H_2−2Zr, it is accompanied by a charge density loss within the B−H bond, lengthening it to 1.25 Å (2150 cm^{-1}) from 1.20 Å (2564 cm^{-1}) and giving it the lowest B−H bond strength of 4.43 eV/bond for the BH and B_2H_2 systems.

The comparison of calculated and experimental frequencies favors a mix of BH and B_2H_2, with the latter capable of forming B−H---Zr bonds, which the former cannot. While the formation energy of 2BH units relative to B_2H_2 shows that BH units are preferable to B_2H_2 (see Table 4), the B_2H_2 unit gains a significant amount of charge density directly between the boron atoms, leading to the greatest total bonding strength. The B−H---Zr interactions are responsible for red-shifting the B−H stretching frequency to ∼2150 cm^{-1}, but due to the lowered total bonding strength and formation energy of B_2H_2−2Zr relative to B_2H_2, this must occur primarily due to high coverages of Zr and B_2H_2. Lastly, identification of adsorbed B_2H_2 and B_2H_2−2Zr as intermediates is supported by their lower energetic stability relative to separated BH units, while their heightened bonding strength with the introduction of B−B bonding forcing hydrogen into closer distances with the

https://doi.org/10.1021/acs.jpcc.4c02327
J. Phys. Chem. C 2024, 128, 12414−12426

Pd(111) and Zr may lead to a lower energetic pathway for the final B−H bond dissociation.

4. DISCUSSION

The numerous past studies that have used $Zr(BH_4)_4$ as a CVD precursor have not addressed the surface chemistry of its decomposition in detail. As a single-source precursor, the molecule would be expected to decompose according to eq 1 upon annealing after condensing an intact molecular layer. Adsorbing $Zr(BH_4)_4$ on Pd(111) at 90 K clearly results in nondissociative adsorption as the RAIR spectrum is identical to that of the molecular solid. The XPS results of Figure 5 for the multilayer at 90 K reveals Zr 3d and B 1s peaks of comparable intensity. Whereas no RAIRS peaks are visible after annealing to 350 K and above, the XPS results indicate Zr remains on the surface after annealing to 600 K. Unfortunately, the XPS sensitivity was insufficient to determine the precise B/Zr ratio after the 600 K anneal. The Zr binding energy shift with annealing to reach a final value after the 600 K anneal of 182 eV, is consistent with, but not definitive proof of, ZrB_2 formation.

The decrease in the RAIRS peak intensities following the 150 K anneal without significant shifts in peak positions indicates molecular desorption without decomposition. However, upon annealing to 200 K the most intense peak in the $Zr(BH_4)_4$ multilayer at 1228 cm^{-1} completely disappears as do the peaks at 1286 and 1053 cm^{-1}. These peaks are all associated with H−B−H bending modes. The two peaks that remain at 2563 and 2153 cm^{-1} are unambiguously assigned to terminal and bridging B−H stretches. Further annealing causes these peaks to red-shift as they decrease in intensity. We attribute the red-shift to a coverage decrease of the responsible surface intermediate as vibrational coupling effects can result in coverage-dependent shifts of a similar magnitude. The loss of all peaks after annealing to 350 K and above contrasts with desorption of H_2 at 426 K. This indicates that H-containing surface intermediates do not give rise to RAIRS peaks of sufficient intensity to be detected. Based on the computational results, we assume that this surface intermediate is B_2H_2. Given that two B atoms and all 16 hydrogen atoms must be removed to convert $Zr(BH_4)_4$ to ZrB_2, the 425 K H_2 desorption peak implies that CVD must be done at or above 426 K.

In a previous study, Sung et al. used an IR multiple-internal reflection technique to detect surface species after exposure of $Zr(BH_4)_4$ to a 1040 nm thick oxide film on a Si(100) surface held at 250 °C.[9] They observed two broad peaks at 2608 and 1148 cm^{-1}, which they tentatively assigned to the B−H stretch and H−B−H bend of a BH_2 surface species. They then concluded that for growth conditions that led to excess boron, the boron was present as BH_2. Their observation that films with excess boron readily oxidized when exposed to air was attributed to the high reactivity of surface BH_2 groups. They found that stoichiometric ZrB_2 films could be readily formed at temperatures as low as 300 °C when atomic hydrogen generated by a microwave plasma was added to the $Zr(BH_4)_4$ flux. The IR peaks assigned to BH_2 were not observed for the stoichiometric ZrB_2 films, which were resistant to oxidation.

As noted by Sung et al., the stoichiometry of diboride films is quite important in determining their properties. In their study they found that thermal CVD using $Zr(BH_4)_4$ on a Si(100) surface at 250−450 °C resulted in films with B/Zr ratios near 3.[9] However, they used relatively low growth temperatures as their goal was to produce amorphous films. In contrast, Tolle et al. used a growth temperature of 900 °C to form crystalline ZrB_2 films on Si(111) from $Zr(BH_4)_4$.[75] Although they did not specifically address the stoichiometry of their film, TEM and XRD results indicated ZrB_2 films of high crystallinity. In latter studies by the same researchers, ZrB_2 films on Si(111) were characterized by XPS, mainly to demonstrate that the films were free of contamination.[32,33] A comparison of their XPS results with our spectra[46,70] from ZrB_2(0001) single crystals indicate that while the Zr 3d and B 1s binding energies are in good agreement, their B 1s/Zr 3d peak area ratios are somewhat larger than in our single crystal results. However, as noted earlier it is difficult to use XPS to accurately determine composition. In a study of HfB_2 films grown on Si(100) using $Hf(BH_4)_4$, Jayaraman et al. concluded that thermal CVD yielded stoichiometric films based on ex situ XPS measurements using literature sensitivity factors, although as expected with XPS the error bars were large, implying a stoichiometry of $HfB_{2\pm0.5}$.[10] Given the importance of obtaining stoichiometric diboride films from $M(BH_4)_4$ precursors, there is clearly a need for a more accurate way to determine the B/M ratios, which would allow the growth conditions to be optimized to produce diboride films with the most desirable properties.

The computational results are clear that a stable BH species forms on Pd(111) from the decomposition of $Zr(BH_4)_4$ and that once formed, two BH molecules can dimerize to form a stable B_2H_2 species. The latter species can form B−H---Zr bridge bonds to one or two Zr atoms. The good match with the experimental RAIRS results in which only bridging and terminal B−H stretches are observed is only consistent with the presence of a B_2H_2 surface intermediate with one or both ends interacting with a Zr atom. The formation of such a three-center two-electron bond for a surface intermediate is not seen in the more widely studied hydrocarbon species on transition metal surfaces. The identification of such a species demonstrates that the unique bonding attributes of boron−hydrogen compounds also pertains to the surface chemistry of metalloboranes such as $Zr(BH_4)_4$.

The computational results also provide insights into the XPS data. Although the signal-to-noise ratios are quite poor, upon adsorption at 90 K, the Zr 3d and B 1s peaks consist of single components indicative of one chemical environment for both atoms as expected for molecular adsorption of $Zr(BH_4)_4$. However, a second binding environment is introduced as the temperature is raised to 200 and 300 K. This is consistent with the computational results implying a mix of Zr not interacting with H or B, and Zr interacting with B_2H_2 through B−H---Zr bridge bonding. Two distinct B 1s peaks would also be expected for BH and B_2H_2.

5. CONCLUSIONS

Zirconium borohydride, $Zr(BH_4)_4$, molecularly adsorbs on Pd(111) at 90 K to yield an infrared spectrum nearly identical to that of solid $Zr(BH_4)_4$. The molecule remains intact after annealing the surface to 150 K, but further annealing to 200 K leads to decomposition to form a surface intermediate that retains terminal and bridging B−H bonds. The computational results reveal that BH is a stable intermediate with a calculated terminal B−H stretch frequency in the range observed experimentally. Once BH is formed, two BH molecules can combine to form a B_2H_2 molecule, as indicated through the energetics, charges, and bonding strengths from the DFT calculations. One or both ends of a B_2H_2 molecule can form B−H---Zr bridge bonds, which further stabilizes the B−B bond

https://doi.org/10.1021/acs.jpcc.4c02327
J. Phys. Chem. C 2024, 128, 12414−12426

of adsorbed B_2H_2. The calculated bridging hydrogen stretching frequency matches the experimental frequency. Identification of such an adsorbed species indicates that the prevalence of three-center two-electron bridge bonding in the chemistry of boron also applies to the surface chemistry of boranes. While XPS results are inconclusive as to whether annealing a condensed $Zr(BH_4)_4$ layer to higher temperatures leads to formation of a ZrB_2 layer, exposure of the Pd(111) surface at 773 K does produce a zirconium diboride film, with a stoichiometry of $ZrB_{1.7\pm0.3}$.

■ ASSOCIATED CONTENT

Supporting Information

The Supporting Information is available free of charge at https://pubs.acs.org/doi/10.1021/acs.jpcc.4c02327.

Adsorbed structures and charge density difference (CDD) isosurfaces, reaction profile of $Zr(BH_4)_1$ and entire $Zr(BH_4)_4$ decomposition, computed energies, charges, and bond lengths, computed infrared spectroscopy, crystal overlap Hamiltonian populations (COHP), first-principles molecular dynamics at 200 K, and VASP coordinates (PDF)

■ AUTHOR INFORMATION

Corresponding Authors

Daniel P. Miller − *Department of Chemistry, Hofstra University, Hempstead, New York 11549, United States;* orcid.org/0000-0003-1507-2667; Email: Daniel.P.Miller@hofstra.edu

Michael Trenary − *Department of Chemistry, University of Illinois Chicago, Chicago, Illinois 60607, United States;* orcid.org/0000-0003-1419-9252; Email: mtrenary@uic.edu

Authors

Ravi Ranjan − *Department of Chemistry, University of Illinois Chicago, Chicago, Illinois 60607, United States;* orcid.org/0000-0003-3755-4704

Morgan Redington − *Department of Chemistry, State University of New York at Buffalo, Buffalo, New York 14260, United States;* orcid.org/0000-0002-5322-2585

Ayoyele Ologun − *Department of Chemistry, University of Illinois Chicago, Chicago, Illinois 60607, United States;* orcid.org/0000-0003-0978-5951

Eva Zurek − *Department of Chemistry, State University of New York at Buffalo, Buffalo, New York 14260, United States;* orcid.org/0000-0003-0738-867X

Complete contact information is available at: https://pubs.acs.org/10.1021/acs.jpcc.4c02327

Notes

The authors declare no competing financial interest.

■ ACKNOWLEDGMENTS

We gratefully acknowledge financial support from the National Science Foundation (DMR-2119308, DMR-2119065, and CNS-2320735). We thank Ms. Connly Yan for help with the $Zr(BH_4)_4$ synthesis. Calculations were performed at the Center for Computational Research at SUNY Buffalo (http://hdl.handle.net/10477/79221) and at Hofstra University. DPM acknowledges computational support from Toon-Chien Wong, Sandesh Goolsarran, Marcus Terry, Alex Fertmann, Alexander Rosenberg, and Mani Tofigh. The authors thank Xiaoyu Wang for helpful discussions pertaining to the FPMD computations.

■ REFERENCES

(1) George, S. M. Atomic layer deposition: An overview. *Chem. Rev.* **2010**, *110*, 111−131.

(2) Zaera, F. The surface chemistry of atomic layer depositions of solid thin films. *J. Phys. Chem. Lett.* **2012**, *3*, 1301−1309.

(3) Zaera, F. Mechanisms of surface reactions in thin solid film chemical deposition processes. *Coord. Chem. Rev.* **2013**, *257*, 3177−3191.

(4) Yao, Y. X.; Coyle, J. P.; Barry, S. T.; Zaera, F. Effect of the nature of the substrate on the surface chemistry of atomic layer deposition precursors. *J. Chem. Phys.* **2017**, *146*, No. 052806, DOI: 10.1063/1.4966201.

(5) Barry, S. T.; Teplyakov, A. V.; Zaera, F. The chemistry of inorganic precursors during the chemical deposition of films on solid surfaces. *Acc. Chem. Res.* **2018**, *51*, 800−809.

(6) Wayda, A. L.; Schneemeyer, L. F.; Opila, R. L. Low-temperature deposition of zirconium and hafnium boride films by thermal decomposition of the metal borohydrides ($M[BH_4]_4$). *Appl. Phys. Lett.* **1988**, *53*, 361−363.

(7) Rice, G. W.; Woodin, R. L. Zirconium Borohydride as a Zirconium Boride Precursor. *J. Am. Ceram. Soc.* **1988**, *71*, C-181−C-183, DOI: 10.1111/j.1151-2916.1988.tb05867.x.

(8) Jensen, J. A.; Gozum, J. E.; Pollina, D. M.; Girolami, G. S. Titanium, zirconium, and hafnium tetrahydroborates as "tailored" CVD precursors for metal diboride thin films. *J. Am. Chem. Soc.* **1988**, *110*, 1643−1644.

(9) Sung, J.; Goedde, D. M.; Girolami, G. S.; Abelson, J. R. Remote-plasma chemical vapor deposition of conformal ZrB_2 films at low temperature: A promising diffusion barrier for ultralarge scale integrated electronics. *J. Appl. Phys.* **2002**, *91*, 3904−3911.

(10) Jayaraman, S.; Yang, Y.; Kim, D. Y.; Girolami, G. S.; Abelson, J. R. Hafnium diboride thin films by chemical vapor deposition from a single source precursor. *J. Vac. Sci. Technol. A* **2005**, *23*, 1619−1625.

(11) Jayaraman, S.; Gerbi, J. E.; Yang, Y.; Kim, D. Y.; Chatterjee, A.; Bellon, P.; Girolami, G. S.; Chevalier, J. P.; Abelson, J. R. HfB_2 and Hf-B-N hard coatings by chemical vapor deposition. *Surf. Coat. Technol.* **2006**, *200*, 6629−6633.

(12) Yang, Y.; Jayaraman, S.; Kim, D. Y.; Girolami, G. S.; Abelson, J. R. CVD growth kinetics of HfB_2 thin films from the single-source precursor $Hf(BH_4)_4$. *Chem. Mater.* **2006**, *18*, 5088−5096.

(13) Yang, Y.; Jayaraman, S.; Kim, D. Y.; Girolami, G. S.; Abelson, J. R. Crystalline texture in hafnium diboride thin films grown by chemical vapor deposition. *J. Cryst. Growth* **2006**, *294*, 389−395.

(14) Yang, Y.; Jayaraman, S.; Sperling, B.; Kim, D. Y.; Girolami, G. S.; Abelson, J. R. In situ spectroscopic ellipsometry analyses of hafnium diboride thin films deposited by single-source chemical vapor deposition. *J. Vac. Sci. Technol. A* **2007**, *25*, 200−206.

(15) Ye, W.; Martin, P. A. P.; Kumar, N.; Daly, S. R.; Rockett, A. A.; Abelson, J. R.; Girolami, G. S.; Lyding, J. W. Direct writing of sub-5 nm hafnium diboride metallic nanostructures. *ACS Nano* **2010**, *4*, 6818−6824.

(16) Nguyen, D.; Mallek, J.; Cloud, A. N.; Abelson, J. R.; Girolami, G. S.; Lyding, J.; Gruebele, M. The energy landscape of glassy dynamics on the amorphous hafnium diboride surface. *J. Chem. Phys.* **2014**, *141*, No. 204501.

(17) Kumar, N.; Noh, W.; Daly, S. R.; Girolami, G. S.; Abelson, J. R. Low temperature chemical vapor deposition of hafnium nitride-boron nitride nanocomposite films. *Chem. Mater.* **2009**, *21*, 5601−5606.

(18) Arpin, K. A.; Losego, M. D.; Cloud, A. N.; Ning, H.; Mallek, J.; Sergeant, N. P.; Zhu, L.; Yu, Z.; Kalanyan, B.; Parsons, G. N.; et al. Three-dimensional self-assembled photonic crystals with high temperature stability for thermal emission modification. *Nat. Commun.* **2013**, *4*, 2630.

(19) Abelson, J. R. Ultra-Conformal CVD at Low Temperatures: The Role of Site Blocking and the Use of Growth Inhibitors. *ECS Trans.* **2010**, *33*, 307−319.

(20) Mitterer, C. Borides in thin film technology. *J. Solid State Chem.* **1997**, *133*, 279−291.
(21) Choi, J. H.; Mao, Y.; Chang, J. P. Development of hafnium based high-k materials—A review. *Mater. Sci. Eng. R* **2011**, *72*, 97−136.
(22) Silvestroni, L.; Kleebe, H.-J.; Fahrenholtz, W. G.; Watts, J. Super-strong materials for temperatures exceeding 2000 °C. *Sci. Rep.* **2017**, *7*, No. 40730.
(23) Nagamatsu, J.; Nakagawa, N.; Muranaka, T.; Zenitani, Y.; Akimitsu, J. Superconductivity at 39 K in magnesium diboride. *Nature* **2001**, *410*, 63−64.
(24) Cumberland, R. W.; Weinberger, M. B.; Gilman, J. J.; Clark, S. M.; Tolbert, S. H.; Kaner, R. B. Osmium Diboride, An Ultra-Incompressible Hard Material. *J. Am. Chem. Soc.* **2005**, *127*, 7264−7265.
(25) Yang, J.; Sun, H.; Chen, C. Is Osmium Diboride An Ultra-Hard Material? *J. Am. Chem. Soc.* **2008**, *130*, 7200−7201.
(26) Hu, C. W.; Chizmeshya, A. V. G.; Tolle, J.; Kouvetakis, J.; Tsong, I. S. T. Nucleation and growth of epitaxial ZrB_2(0001) on Si(111). *J. Cryst. Growth* **2004**, *267*, 554−563.
(27) Tolle, J.; Kouvetakis, J.; Kim, D. W.; Mahajan, S.; Bell, A.; Ponce, F. A.; Tsong, I. S. T.; Kottke, M. L.; Chen, Z. H. D. Epitaxial growth of $Al_xGa_{1-x}N$ on Si(111) via a ZrB_2(0001) buffer layer. *Appl. Phys. Lett.* **2004**, *84*, 3510−3512.
(28) Liu, P. L.; Chizmeshya, A. V. G.; Kouvetakis, J.; Tsong, I. S. T. First-principles studies of GaN(0001) heteroepitaxy on ZrB_2(0001). *Phys. Rev. B* **2005**, *72*, No. 245335.
(29) Roucka, R.; Tolle, J.; Chizmeshya, A. V. G.; Tsong, I. S. T.; Kouvetakis, J. Epitaxial film growth of zirconium diboride on Si(001). *J. Cryst. Growth* **2005**, *277*, 364−371.
(30) Tolle, J.; Kouvetakis, J.; Kim, D. W.; Mahajan, S.; Chizmeshya, A. V. G.; Hu, C. W.; Bell, A.; Ponce, F. A.; Tsong, I. S. T. Epitaxial growth of ZrB_2(0001) on Si(111) for III-nitride applications: A review. *Chin. J. Phys.* **2005**, *43*, 233−248.
(31) Trivedi, R.; Liu, P. L.; Roucka, R.; Tolle, J.; Chizmeshya, A. V. G.; Tsong, I. S. T.; Kouvetakis, J. Mismatched heteroepitaxy of tetrahedral semiconductors with Si via ZrB_2 templates. *Chem. Mater.* **2005**, *17*, 4647−4652.
(32) Yamada Takamura, Y.; Wang, Z. T.; Fujikawa, Y.; Sakurai, T.; Xue, Q. K.; Tolle, J.; Liu, P.-L.; Chizmeshya, A. V. G.; Kouvetakis, J.; Tsong, I. S. T. Surface and Interface Studies of GaN Epitaxy on Si(111) via ZrB_2 Buffer Layers. *Phys. Rev. Lett.* **2005**, *95*, No. 266105.
(33) Wang, Z. T.; Yamada-Takamura, Y.; Fujikawa, Y.; Sakurai, T.; Xue, Q. K.; Tolle, J.; Kouvetakis, J.; Tsong, I. S. T. Effect of nitridation on the growth of GaN on ZrB_2(0001)/Si(111) by molecular-beam epitaxy. *J. Appl. Phys.* **2006**, *100*, No. 033506.
(34) Blake, A. H.; Caselli, D.; Durot, C.; Mueller, J.; Parra, E.; Gilgen, J.; Boley, A.; Smith, D. J.; Tsong, I. S. T.; Roberts, J. C. InGaN/GaN multiple-quantum-well light-emitting diodes grown on Si(111) substrates with ZrB_2(0001) buffer layers. *J. Appl. Phys.* **2012**, *111*, No. 033107, DOI: 10.1063/1.3684557.
(35) Prokvolit, S.; Mao, E.; Gray, T. G. Early events in the mechanism of single-source chemical vapor deposition of zirconium and hafnium diboride: a computational investigation. *Phys. Chem. Chem. Phys.* **2024**, *26*, 1217−1224.
(36) Walkosz, W.; Manandhar, K.; Trenary, M.; Otani, S.; Zapol, P. Dissociative adsorption of hydrogen on the ZrB_2(0001) surface. *Surf. Sci.* **2012**, *606*, 1808−1814.
(37) Manandhar, K.; Trenary, M.; Otani, S.; Zapol, P. Dissociation of trimethylgallium on the ZrB_2(0001) surface. *J. Vac. Sci. Technol., A* **2013**, *31*, No. 061405.
(38) Manandhar, K.; Walkosz, W.; Ren, Y.; Otani, S.; Zapol, P.; Trenary, M. Structure and reactivity of molecularly adsorbed ammonia on the ZrB_2(0001) surface. *J. Phys. Chem. C* **2014**, *118*, 29260−29269.
(39) Housecroft, C. E.; Fehlner, T. P. Metalloboranes - Their Relationship to Metal Hydrocarbon Complexes and Clusters. *Adv. Organometal. Chem.* **1982**, *21*, 57−112.
(40) Greenwood, N. N. Metalloboranes and metal-boron bonding. *Chem. Soc. Rev.* **1974**, *3*, 231−271.
(41) Greenwood, N. N. Metalloboranes. *Pure Appl. Chem.* **1983**, *55*, 1415−1430.
(42) Housecroft, C. E. *Boranes and Metalloboranes*; Ellis Horwood: Chichester, 1990.
(43) Borthakur, R.; Saha, K.; Kar, S.; Ghosh, S. Recent advances in transition metal diborane(6), diborane(4) and diborene(2) chemistry. *Coord. Chem. Rev.* **2019**, *399*, No. 213021.
(44) Feng, X.; Abdel-Rahman, M. K.; Kruppe, C. M.; Trenary, M. Deposition and characterization of stoichiometric films of V_2O_5 on Pd(111). *Surf. Sci.* **2017**, *664*, 1−7.
(45) Kang, D. H.; Trenary, M. Surface Chemistry of Ethylenediamine ($NH_2CH_2CH_2NH_2$) on Pt(111). *Surf. Sci.* **2000**, *470*, L13−L19.
(46) Manandhar, K.; Walkosz, W.; Trenary, M.; Otani, S.; Zapol, P. Dissociative adsorption of ammonia on the ZrB_2(0001) surface. *Surf. Sci.* **2013**, *615*, 110−118.
(47) Davies, N.; Saunders, D.; Wallbridge, M. G. H. Exchange reactions of zirconium tetrakistetrahydroborate. *J. Chem. Soc. A* **1970**, 2915 DOI: 10.1039/J19700002915.
(48) Haaland, A.; Shorokhov, D. J.; Tutukin, A. V.; Volden, H. V.; Swang, O.; Mcgrady, G. S.; Kaltsoyannis, N.; Downs, A. J.; Tang, C. Y.; Turner, J. F. C. Molecular Structures of Two Metal Tetrakis-(tetrahydroborates), $Zr(BH_4)_4$ and $U(BH4)_4$: Equilibrium Conformations and Barriers to Internal Rotation of the Triply Bridging BH_4 Groups. *Inorg. Chem.* **2002**, *41*, 6646−6655.
(49) Marks, T. J.; Kolb, J. R. Covalent transition metal, lanthanide, and actinide tetrahydroborate complexes. *Chem. Rev.* **1977**, *77*, 263−293.
(50) Gennari, F. C.; Fernández Albanesi, L.; Rios, I. J. Synthesis and thermal stability of $Zr(BH_4)_4$ and $Zr(BD_4)_4$ produced by mechanochemical processing. *Inorg. Chim. Acta* **2009**, *362*, 3731−3737.
(51) Volkov, V. V.; Sobolev, E. V.; Zaev, E. E.; Shapiro, O. I. Ir and PMR spectra and structure of zirconium and hafnium borohydrides. *J. Struct. Chem.* **1968**, *8*, 407−409.
(52) Rude, L. H.; Corno, M.; Ugliengo, P.; Baricco, M.; Lee, Y.-S.; Cho, Y. W.; Besenbacher, F.; Overgaard, J.; Jensen, T. R. Synthesis and Structural Investigation of $Zr(BH_4)_4$. *J. Phys. Chem. C* **2012**, *116*, 20239−20245.
(53) Ko, E. I.; Benziger, J. B.; Madix, R. J. Reactions of methanol on W(100) and W(100)-(5 × 1)C surfaces. *J. Catal.* **1980**, *62*, 264−274.
(54) Summers, R. L. *Empirical Observations on the Sensitivity of Hot Cathode Ionization Type Vacuum Gauges*; Rep. no. NASA-TN-D-5285; NASA, Ed., 1969.
(55) Kresse, G.; Furthmüller, J. Efficient iterative schemes for ab initio total-energy calculations using a plane-wave basis set. *Phys. Rev. B* **1996**, *54*, 11169.
(56) Klimeš, J.; Bowler, D. R.; Michaelides, A. Chemical accuracy for the van der Waals density functional. *J. Phys.: Condens. Matter* **2010**, *22*, No. 022201.
(57) Klimeš, J.; Bowler, D. R.; Michaelides, A. Van der Waals density functionals applied to solids. *Phys. Rev. B* **2011**, *83*, No. 195131.
(58) Henkelman, G.; Uberuaga, B. P.; Jónsson, H. A climbing image nudged elastic band method for finding saddle points and minimum energy paths. *J. Chem. Phys.* **2000**, *113*, 9901−9904.
(59) Henkelman, G.; Jónsson, H. Improved tangent estimate in the nudged elastic band method for finding minimum energy paths and saddle points. *J. Chem. Phys.* **2000**, *113*, 9978−9985.
(60) Blöchl, P. E. Projector Augmented-Wave Method. *Phys. Rev. B* **1994**, *50*, 17953−17979.
(61) Kresse, G.; Joubert, D. From ultrasoft pseudopotentials to the projector augmented-wave method. *Phys. Rev. B* **1999**, *59*, 1758.
(62) Schwarzer, M.; Hertl, N.; Nitz, F.; Borodin, D.; Fingerhut, J.; Kitsopoulos, T. N.; Wodtke, A. M. Adsorption and Absorption Energies of Hydrogen with Palladium. *J. Phys. Chem, C* **2022**, *126*, 14500−14508.

(63) Nosé, S. A unified formulation of the constant temperature molecular dynamics methods. *J. Chem. Phys.* **1984**, *81*, 511−519.
(64) Hoover, W. G. Canonical dynamics: Equilibrium phase-space distributions. *Phys. Rev. A* **1985**, *31*, 1695−1697.
(65) Maintz, S.; Deringer, V. L.; Tchougréeff, A. L.; Dronskowski, R. LOBSTER: A tool to extract chemical bonding from plane-wave based DFT. *J. Comput. Chem.* **2016**, *37*, 1030−1035.
(66) Frisch, M. J.; Trucks, G. W.; Schlegel, H. B.; Scuseria, G. E.; Robb, M. A.; Cheeseman, J. R.; Scalmani, G.; Barone, V.; Petersson, G. A.; Nakatsuji, H. *Gaussian 16 rev.*; Gaussian Inc.: Wallingford, CT, USA, 2016.
(67) Smith, B. E.; Shurvell, H. F.; James, B. D. Molecular vibrations of zirconium(IV) tetrahydroborate, a compound containing triple hydrogen bridges. *J. Chem. Soc., Dalton Trans.* **1978**, 710.
(68) Davies, N.; Wallbridge, M. G. H.; Smith, B. E.; James, B. D. Vibrational spectra of zirconium tetrahydroborate and related molecules. *J. Chem. Soc., Dalton Trans.* **1973**, 162.
(69) Tahir, D.; Suarga, S.; Yulianti, Y.; Sari, N. H. Stopping Powers and Inelastic Mean Free Path of 100 eV to 30 keV Electrons in Zirconium Silicates. *Atom Indonesia* **2013**, *38*, 100.
(70) Singh, R.; Trenary, M.; Paderno, Y. Analysis of a zirconium diboride single crystal, $ZrB_2(0001)$, by XPS. *Surf. Sci. Spectra* **2000**, *7*, 310−316.
(71) Weng, L. T.; Vereecke, G.; Genet, M. J.; Rouxhet, P. G.; Stone-Masui, J. H.; Bertrand, P.; Stone, W. E. E.; Part, II. Quantitative XPS. Part II: Comparison Between Quantitative Approaches for Two Different Spectrometers — Determination of the Contamination-Reduced Thickness, Application of the Determined Transmission Functions and Accuracy Achieved. *Surf. Interface Anal.* **1993**, *20*, 193−205.
(72) Otani, S.; Ishizawa, Y. Preparation of ZrB_2 single crystals by the floating zone method. *J. Cryst. Growth* **1996**, *165*, 319−322.
(73) Moulder, J. F.; Stickle, W. F.; Sobol, P. E.; Bomben, K. D. *Handbook of X-ray Photoelectron Spectroscopy*; Perkin-Elmer Corporation: MN, 1992.
(74) Hedberg, K.; Plato, V. Electron-diffraction investigation of zirconium tetraborohydride, $Zr(BH_4)_4$. *Inorg. Chem.* **1971**, *10*, 590−594.
(75) Tolle, J.; Roucka, R.; Tsong, I. S. T.; Ritter, C.; Crozier, P. A.; Chizmeshya, A. V. G.; Kouvetakis, J. Epitaxial growth of group III nitrides on silicon substrates via a reflective lattice-matched zirconium diboride buffer layer. *Appl. Phys. Lett.* **2003**, *82*, 2398−2400.

https://doi.org/10.1021/acs.jpcc.4c02327
J. Phys. Chem. C 2024, 128, 12414−12426